

**LEVEL**

**2**

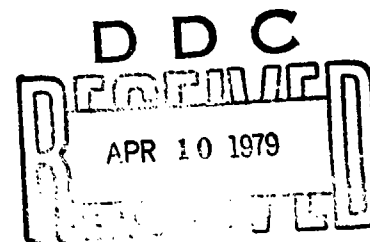
**AFATL-TR-78-117**

**Morphological Characteristics of  
Particulate Material Formed from  
High Velocity Impact of Depleted  
Uranium Projectiles with Armor  
Targets**

**ENVIRONICS OFFICE**

**NOVEMBER 1978**

**FINAL REPORT FOR PERIOD OCTOBER 1977-OCTOBER 1978**



*90*

*C*

Approved for public release; distribution unlimited



**Air Force Armament Laboratory**

**AIR FORCE SYSTEMS COMMAND • UNITED STATES AIR FORCE • EGLIN AIR FORCE BASE, FLORIDA**

**79 04 04 04 9**

**DDC FILE COPY AD A0 67121**

UNCLASSIFIED

SECURITY CLASSIFICATION OF THIS PAGE (When Data Entered)

| REPORT DOCUMENTATION PAGE  |   | READ INSTRUCTIONS<br>BEFORE COMPLETING FORM          |  |
|--|---|--|--|
| 1. REPORT NUMBER<br>AFATL-TR-78-117  | 2. GOVT ACCESSION NO.   | 3. RECIPIENT'S CATALOG NUMBER                        |  |
| 4. TITLE (and Subtitle)<br>MORPHOLOGICAL CHARACTERISTICS OF PARTICULATE<br>MATERIAL FORMED FROM HIGH VELOCITY IMPACT OF<br>DEPLETED URANIUM PROJECTILES WITH ARMOR TARGETS   | 5. AUTHOR(s)<br>Michael A./Patrick Capt, USAF, Ph.D.<br>J. C./Cornette, Ph.D.                               | 6. CONTRACT OR GRANT NUMBER(s)                       | 7. PERFORMING ORG. REPORT NUMBER             |
| 8. PERFORMING ORGANIZATION NAME AND ADDRESS<br>Envionics Office<br>Air Force Armament Laboratory<br>Eglin Air Force Base, Florida 32542  | 9. PROGRAM ELEMENT, PROJECT, TASK<br>AREA & WORK UNIT NUMBERS<br>JON: 06CD-01-01<br>Program Element: 62502F | 10. REPORT DATE<br>November 1978                     | 11. NUMBER OF PAGES<br>28                    |
| 12. CONTROLLING OFFICE NAME AND ADDRESS<br>Air Force Armament Laboratory<br>Armament Development and Test Center<br>Eglin Air Force Base, Florida 32542  | 13. MONITORING AGENCY NAME & ADDRESS (if different from Controlling Office)<br>12/28p.                      | 14. SECURITY CLASS. (of this report)<br>UNCLASSIFIED | 15. DECLASSIFICATION/DOWNGRADING<br>SCHEDULE |
| 16. DISTRIBUTION STATEMENT (of this Report)<br><br>Approved for public release; distribution unlimited   |   |  |  |
| 17. DISTRIBUTION STATEMENT (of the abstract entered in Block 20, if different from Report)   |   |  |  |
| 18. SUPPLEMENTARY NOTES<br><br>Available in DDC  |   |  |  |
| 19. KEY WORDS (Continue on reverse side if necessary and identify by block number)<br>Scanning Electron Microscopy    Armor-Piercing Munition<br>Particles    X-Ray Energy Spectroscopy<br>Penetrator    Depleted Uranium<br>GAU-8    Respirable Hazard  |   |  |  |
| 20. ABSTRACT (Continue on reverse side if necessary and identify by block number)<br>Scanning electron microscopy was used to investigate the particles formed when depleted uranium projectiles (99.25 percent depleted uranium, 0.75 percent titanium) impact armor targets. Special emphasis was placed on the morphological characteristics of the particles in relationship to size, crystalline structure, and inherent stability. Airborne particles, which had been collected on cellophane tape, were observed directly following sputter coating. These particles were primarily spherical in shape, indicating formation from |   |  |  |

DD FORM 1 JAN 73 1473 EDITION OF 1 NOV 65 IS OBSOLETE

UNCLASSIFIED

SECURITY CLASSIFICATION OF THIS PAGE (When Data Entered)

400 856


JW

UNCLASSIFIED

SECURITY CLASSIFICATION OF THIS PAGE (When Data Entered)

Item 20: (Concluded) molten material. Crystalline structure was highly variable and was dependent upon the degree of alloying with target material as determined by X-ray energy spectroscopy. The surfaces of these particles were covered to varying extents by large numbers of coalesced, ultrafine ( $<0.1 \mu m$ ) particulates. Soil particles, which were sieved and density separated from debris prior to microscopic examination, consisted of spheres and irregularly shaped fragments. X-ray analysis confirmed alloying and fusion with clay and sand particulates.

micrometers

|   |   |
|---|---|
| COFFSET'S for   |   |
| NTIS  | White Section <input checked="" type="checkbox"/> |
| DOC   | Buff Section <input type="checkbox"/>             |
| HARRISON  |   |
| HISSE   |   |
| DISTRICT  |   |
|  |   |

UNCLASSIFIED

## PREFACE

This report is the result of research conducted by the Air Force Armament Laboratory, Armament Development and Test Center, Eglin Air Force Base, Florida, from October 1977 to October 1978 under Air Force Exploratory Development Project 06CD0101.

Reference to specific manufacturers or suppliers of scientific equipment used in this study is for the sole purpose of identification and does not constitute endorsement of the products by the United States Air Force.

This report has been reviewed by the Information Office (OI) and is releasable to the National Technical Information Service (NTIS). At NTIS, it will be available to the general public, including foreign nations.

This technical report has been reviewed and is approved for publication.

FOR THE COMMANDER

  
JOE A. FARMER  
Chief, Environics Office

## TABLE OF CONTENTS

| Section | Title  | Page |
|---------|--|------|
| I       | INTRODUCTION . . . . .                         | 1    |
| II      | MATERIALS AND METHODS. . . . .                 | 2    |
| III     | RESULTS. . . . .                               | 3    |
|         | Airborne Particles . . . . .                   | 6    |
|         | Particles Isolated from Soil Samples . . . . . | 13   |
|         | Particle Composition . . . . .                 | 13   |
| IV      | TECHNICAL SUMMARY . . . . .                    | 18   |
|         | REFERENCES . . . . .                           | 20   |

## LIST OF FIGURES

| Figure | Title   | Page |
|--------|---|------|
| 1      | Diagram of Firing Site: Ford Farm Firing Range, Aberdeen Proving Ground, MD. . . . .  | 3    |
| 2      | Overhead Diagram of Target . . . . .  | 4    |
| 3      | Typical X-Ray Energy Spectrum Resulting from the Bombardment of a Depleted Uranium and Iron Particle with a 25 kV Electron Beam. . . . .  | 5    |
| 4      | Overall View of Airborne Particles Collected on Double-Stick Tape at Sample Site 3; Bar Represents 55.5 $\mu\text{m}$ . . . . .   | 7    |
| 5      | Dual Magnification (3X) of Airborne Particle Showing Convuluted Surface Pattern and Fusion of Concave Surface Plates; Small Bar Represents 5 $\mu\text{m}$ at Lower Magnification . . . . . | 7    |
| 6      | Dual Magnification (5X) of Airborne Particle Depicting Surface Fracturing; Small Bar Represents 5 $\mu\text{m}$ at Lower Magnification. . . . .   | 9    |
| 7      | Demonstration of Particle Breakup as a Result of Inherent Fragility; Small Bar Represents 5 $\mu\text{m}$ . . . . .   | 9    |
| 8      | Dual Magnification (5X) of Polycrystalline Particle Consisting Primarily of Iron; Small Bar Represents 5 $\mu\text{m}$ at Lower Magnification . . . . .                                     | 10   |
| 9      | Hollow Particle Demonstrating Variable Wall Thickness; Bar Represents 5 $\mu\text{m}$ . . . . .   | 10   |
| 10     | Perforated, Hollow Sphere; Bar at Right Represents 5 $\mu\text{m}$ . . . . .  | 11   |
| 11     | Several Airborne Particles Demonstrating Surface Coverage by Ultrafine Particulates; Bar at Right Represents 5 $\mu\text{m}$ . . . . .  | 11   |
| 12     | Dual Magnification (10X) of a Depleted Uranium and Iron Particle; Bar Represents 55.5 $\mu\text{m}$ at Lower Magnification . . . . .  | 12   |
| 13     | Flaring of an Ultrafine Aggregate from the Surface of an Airborne Particle Shown in Dual Magnification (3X); Bar at Right Represents 5 $\mu\text{m}$ Lower Magnification . . . . .          | 12   |
| 14     | Ultrafine Particulates on the Surface of Depleted Uranium Particles Showing Interconnecting Thread; Bar at Right Represents 5 $\mu\text{m}$ . . . . .                                       | 14   |
| 15     | Concentric Pattern of Free Ultrafine Particulates on Double-Stick Tape; Bar Represents 55.5 $\mu\text{m}$ . . . . .   | 14   |
| 16     | High Magnification Showing Aggregation of Ultrafine Particles; Gap Between Bars Represents 0.5 $\mu\text{m}$ . . . . .  | 15   |

# LIST OF FIGURES (CONCLUDED)

| Figure | Title  | Page |
|--------|--|------|
| 17     | Soil Particles of Density Greater Than 4.3 Which Passed Through a 12 $\mu\text{m}$ Polycarbonate Nuclepore Membrane; Bar Represents 55.5 $\mu\text{m}$ . . . . . | 15   |
| 18     | Dual Magnification (10X) of Soil Particles Revealing Both Spherical Particles and Fragments; Bar Represents 55.5 $\mu\text{m}$ at Lower Magnification . . . . .  | 16   |
| 19     | Knobby Soil Particle; Gap Between Bars Represents 0.5 $\mu\text{m}$ . .  | 16   |
| 20     | Dual Magnification (5X) of Particle Breakup Due to 15-Second Exposure to Ultrasound; Bar Represents 55.5 $\mu\text{m}$ at Lower Magnification . . . . .          | 17   |

v

(The reverse of this page is blank)

## SECTION I

### INTRODUCTION

Development of high-density, armor-piercing munitions has led to widespread use of metallic depleted uranium by the armed services. Notable weapons employing depleted uranium include the Air Force GAU-8, the Army XM 774 and M735E1, and the PHALANX gun systems.

Armor-piercing munitions are specifically designed to defeat armored targets through primary impact of a high-density, nonexplosive core or penetrator. Using depleted uranium as the penetrator material, fire is realized as a secondary damage-mechanism due to the pyrophoric\* nature of the depleted uranium projectile which bursts into burning fragments upon impact with armor. It was the objective of this work to study the nature and formation of these fragments and to describe the particulates which are generated as a result of the physical breakup and the vigorous oxidation of depleted uranium. Scanning electron microscope techniques coupled with energy dispersive X-ray spectroscopy were used to determine the morphological characteristics of the particulate material. Emphasis was placed on determining the size range, crystalline structure, and stability of the resulting particles. Information obtained from this study will be useful in future assessments concerning the impact of depleted uranium munitions on the environment. The data will also be valuable in understanding and providing for protection of personnel associated with testing and operational use of this type of weaponry. It is anticipated that the results of these Aberdeen tests will provide insight in understanding the events which occur during 30 mm testing at Eglin Air Force Base.

---

\*Popular usage of the term pyrophoric has led to its acceptance for describing this high-density metal (depleted uranium) since, at high velocity, it spontaneously ignites and burns upon impact with armor.



## SECTION II

### MATERIALS AND METHODS

Depleted uranium particulate samples studied in this report were obtained following test firings of the Army 105 mm XM 774 antitank round at the Fort Detrick Firing Range, Aberdeen Proving Ground, MD during October 1977. The rounds were test fired against spaced armor targets from a distance of approximately 200 meters. Penetrators consisted of 3.5 kg alloyed depleted uranium containing 0.75 percent titanium by weight. A diagram of the firing site and an overhead view of the target area are shown in Figures 1 and 2 (courtesy of Battelle Pacific Northwest Laboratories), respectively.

Air sample collectors were positioned at three locations adjacent to the target butt; site 1 was directly east and approximately 2 meters above ground level; site 2 was 4 meters south and 2 meters above ground level; and site 3 was 1.5 meters west and 2 meters above ground level. Soil samples were collected directly beneath and behind the target plates.

Airborne particles were collected on double-stick cellophane tape. Cut portions of the tape were placed on carbon coated aluminum stubs (15 mm in diameter) and coated with 100 percent gold in an International Scientific Instrument PS-2 Sputter Coater.

All soil samples were sieved through a 400 mesh (37  $\mu\text{m}$  opening) screen to eliminate large particulate material. Only that fraction which passed through the 400 mesh screen was used for subsequent analyses. Selected samples were passed through a 12  $\mu\text{m}$  pore diameter, hydrophobically treated Nucleopore Membrane, to concentrate particles in the respirable range. Following the sieving operations, samples were centrifuged at 500 rpm in an aqueous solution of thallium formate-thallium malonate (density 4.3). Particles with a density greater than that of the fluid medium were collected at the bottom of the tube. This high density particulate material was then trapped on 0.4  $\mu\text{m}$  pore diameter Nucleopore membranes. After repeated washings with distilled water, the membranes were air dried, placed on carbon coated aluminum stubs, and coated with 100 percent gold as previously described.

Particulate materials were examined in an International Scientific Instrument Super III A Scanning Electron Microscope at an accelerating voltage of 25 kV. Elemental composition of the particles (to 0.5  $\mu\text{m}$  in diameter) was identified with either a Kevex 5500 or Kevex 5100 X-Ray Energy Spectrometer with a detector resolution of 146 eV. Specimen tilt angles varied from a 0- to 45-degree tilt. Uranium was identified by its  $\text{M}\alpha$  and  $\text{M}\beta$  X-ray peaks at 3.17 keV and 3.33 keV, respectively. A typical X-ray spectrum is illustrated in Figure 3. The MLK marker (white bar) identifies the  $\text{M}\alpha$  peak for uranium. Additional peaks represented in the spectrum are aluminum ( $\text{K}\alpha$  1.48 keV), gold ( $\text{M}\alpha$  2.12 keV), titanium ( $\text{K}\alpha$  4.51 keV), and iron ( $\text{K}\alpha$  6.40 keV,  $\text{K}\beta$  7.06 keV).

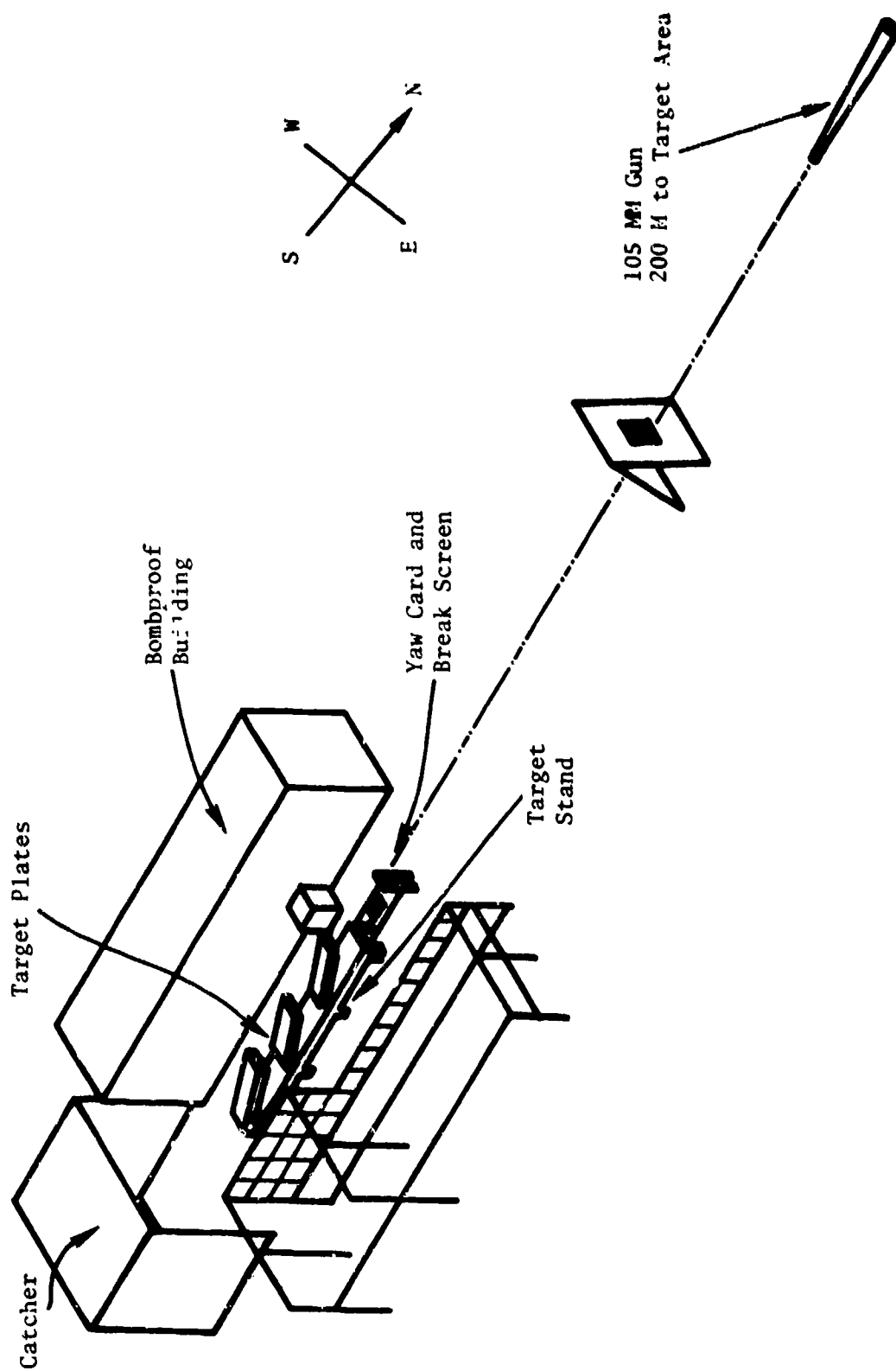


Figure 1. Diagram of Firing Site: Ford Farm Firing Range, Aberdeen Proving Ground, MD

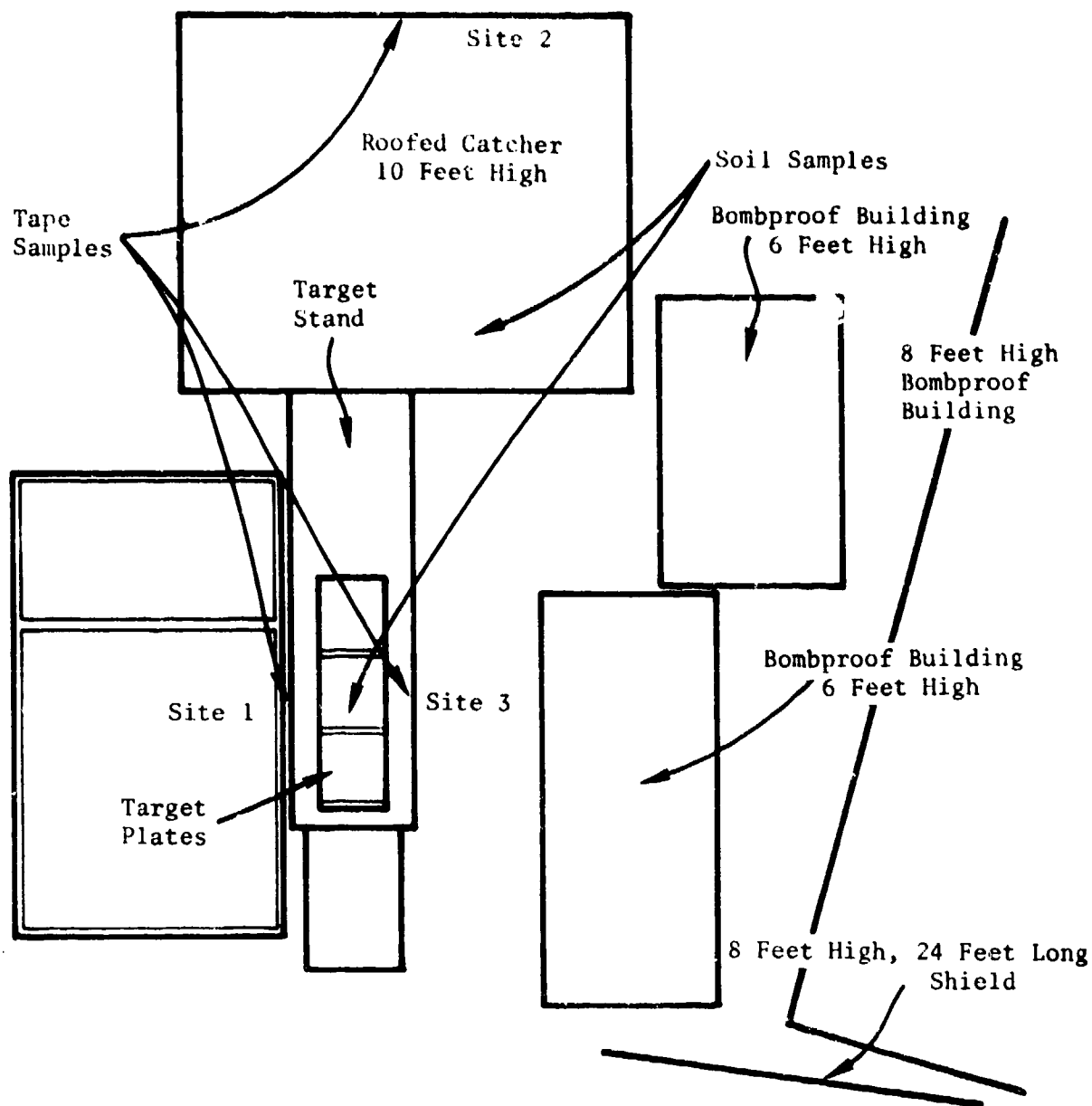


Figure 2. Overhead Diagram of Target Area

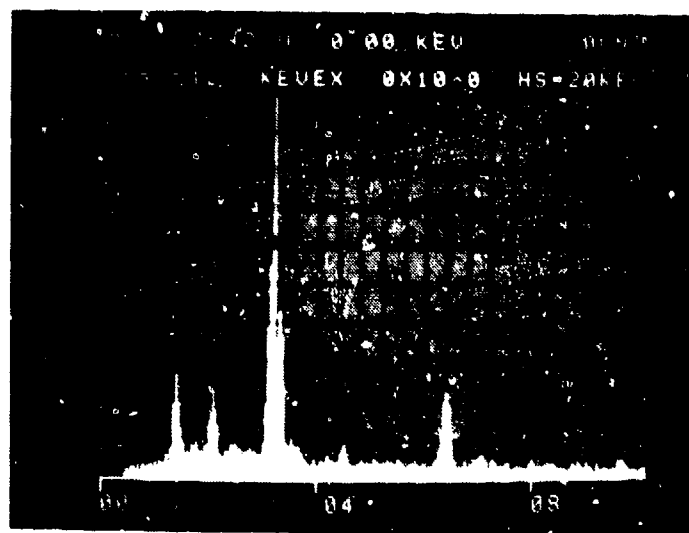


Figure 5. Typical X-Ray Energy Spectrum Resulting from the Bombardment of a Staballoy and Iron Particle with a 25 kV Electron Beam

## SECTION III

### RESULTS

#### AIRBORNE PARTICLES

As shown in Figure 4, impact of 105 mm depleted uranium penetrators against multiple armor plate target resulted in the formation of large numbers of airborne particulates. At this relatively low magnification, it was apparent that particulate material was generated over an extremely broad size range, i.e., from macro fragments at diameters greater than 50  $\mu$ m to submicron particulate aerosols. Other than sheared or broken fragments, most of the particles observed were either spherical or ellipsoidal in shape, indicating sufficient heat generation following impact to cause the formation of molten uranium and uranium oxides. The extreme temperature required for melting, in excess of 1133°C (Reference 1), undoubtedly resulted from the combined effects of frictional forces at impact and oxidation of the pyrophoric penetrator material. During the process of penetration of multiple armor targets, depleted uranium penetrators undergo severe fragmentation. With the type of targets utilized in the study, the only recognizable remaining portion of the original penetrator is normally a small section near the base. Fragments produced are ignited spontaneously by a combination of shock and friction heating at impact. Combustion of fragments in air is exothermic and self-sustaining. Flash temperatures reached during impact of depleted uranium penetrators with armor plate have been shown to fall in the range of 5500 to 5600°F (Reference 2). Test results show further a nearly constant (3037 to 3093°C) impact flash temperature over the entire range of impact velocities from 4010 to 5560 feet per second. Such temperatures, especially in view of the severe penetrator breakup demonstrated by the XM 774, are sufficient to initiate combustion of the numerous particles produced.

Measuring fine particles is generally a cumbersome, if not complex, task. However, due to the nearly spherical shape of most of the particles encountered in this study, direct diameter measurements were relatively simple to perform.

Examination of numerous particles revealed several distinct morphologies. The great majority of airborne particles exhibited a rugose or convoluted structure which frequently appeared, at surface level, to consist of large, interconnecting concave plates (Figure 5). Each plate, formed independently from the solidification of molten material, was observed to radiate from a common origin or focal point upon the surface. At or near the junction of adjacent plates considerable overlapping and fusion occurred, resulting in distinct but irregularly delineated boundary edges. Higher magnification revealed numerous imperfections in the overall crystalline structure along the surface, thereby serving to further subdivide each major plate.

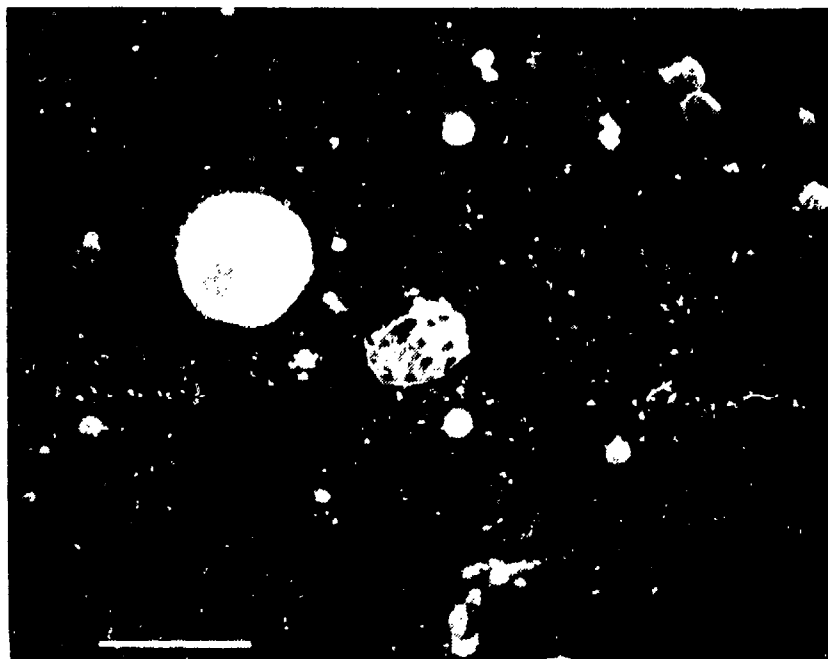


Figure 4. Overall View of Airborne Particles Collected  
on Double-Stick Tape at Sample Site 3;  
Bar Represents 55.5  $\mu\text{m}$

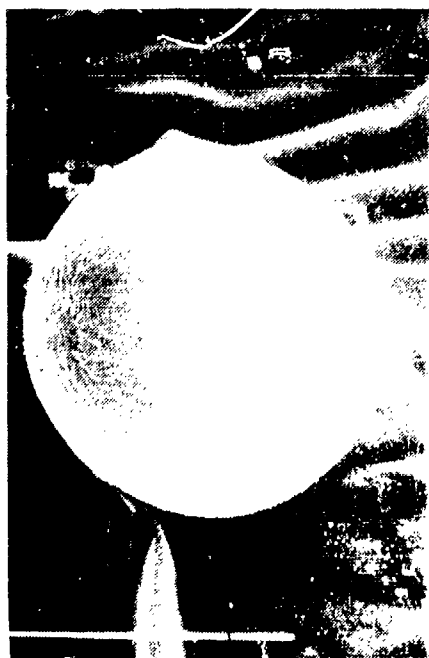


Figure 5. Dual Magnification (3X) of Airborne Particle Showing  
Convoluted Surface Pattern and Fusion of Concave Surface Plates;  
Small Bar Represents 5  $\mu\text{m}$  at Lower Magnification

As illustrated in Figure 6, some rugose particles exhibited a more uniform surface morphology, devoid of major plate divisions. The convoluted surface, although similar to that previously described, consisted of deeper, more numerous folds and extensive dimpling. Fissures and pore-like invaginations were frequently observed and progressively developed into deep fractures, presumably as a consequence of thermal expansion or through collisions with other objects. These fractures, which traversed irregular courses along the convoluted folds, were the eventual cause of extensive particle breakup (Figure 7).

A unique class of particulates, best described as polycrystalline, was frequently found (Figure 8). Only observed at diameters greater than 40  $\mu\text{m}$ , these particles consisted of a tight but irregular mass of nearly cuboidal crystals. Although these particles lacked the orderly and systematic intracrystalline alignment often associated with polycrystalline formations, the net result was the creation of nearly perfect spheres exhibiting relatively smooth but discontinuous surfaces. It should be noted that, when fractured, these particles revealed a similar crystalline structure throughout their solid interiors. X-ray data indicated that these particles contained an extremely high content of iron with relatively small quantities of uranium present.

Internal morphology was frequently revealed by examination of fractured particles, particularly those in which large portions had become detached. Both solid and hollow particles were observed, the latter clearly demonstrated by the presence of hemispherical fragments (Figure 9). Although wall thickness varied greatly, the inner surface morphology of hollow particles consistently resembled that of the outer surface.

Perforated depleted uranium particles, similar in many respects to those reported for fly ash and oil soot (Reference 3), are shown in Figure 10. Some of the particles observed were so highly perforated and thin-walled that impact with the collecting tape resulted in distortion, collapse or complete breakup. The unusual nature of these particles is consistent with the oxidative processes and violent outgassing known to occur during formation of such particles.

Prior to weathering, the surfaces of most airborne particles were covered to a varying extent by immense numbers of nearly spherical, ultrafine particulates less than 0.1  $\mu\text{m}$  in diameter (Figure 11). Identity of these particulates as pure or alloyed uranium was confirmed by X-ray analysis.

An example of the uniform dispersal of ultrafine particulates on the surface of a depleted uranium/iron particle is demonstrated in Figure 12. Any further accumulation, however, generally resulted in extensive coagulation and hence the formation of large billowing aggregates (Figure 13).

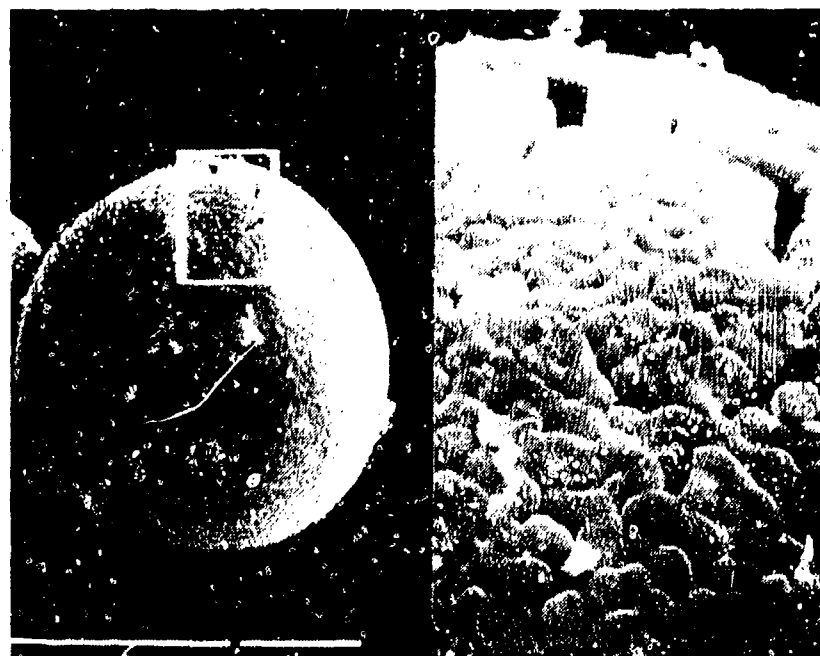


Figure 6. Dual magnification (5X) of Airborne Particle  
 Depicting Surface Fracturing; Small Bar Represents  
 5  $\mu\text{m}$  at Lower Magnification

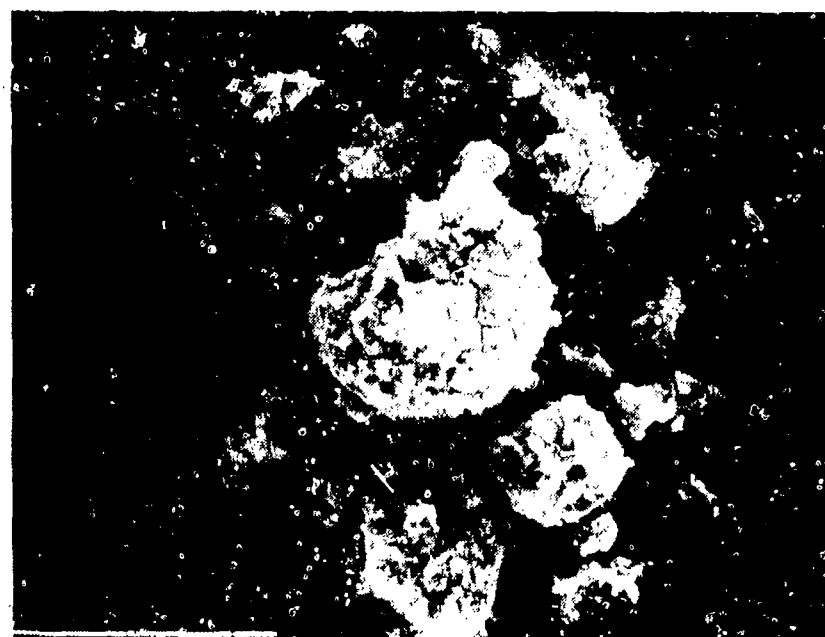
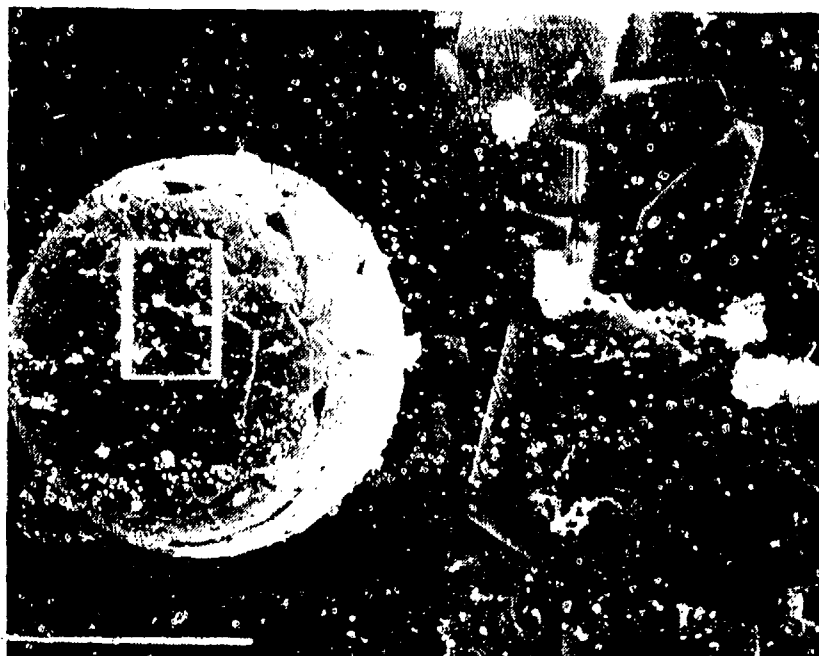


Figure 7. Demonstration of Particle Breakup as a Result  
 of Inherent Fragility; Small Bar Represents 5  $\mu\text{m}$





(Note the ultrafine particulates of depleted uranium adhering to surface)

Figure 8. Dual Magnification (5X) of Polycrystalline Particle Consisting Primarily of Iron; Small Bar Represents 5  $\mu\text{m}$  at Lower Magnification

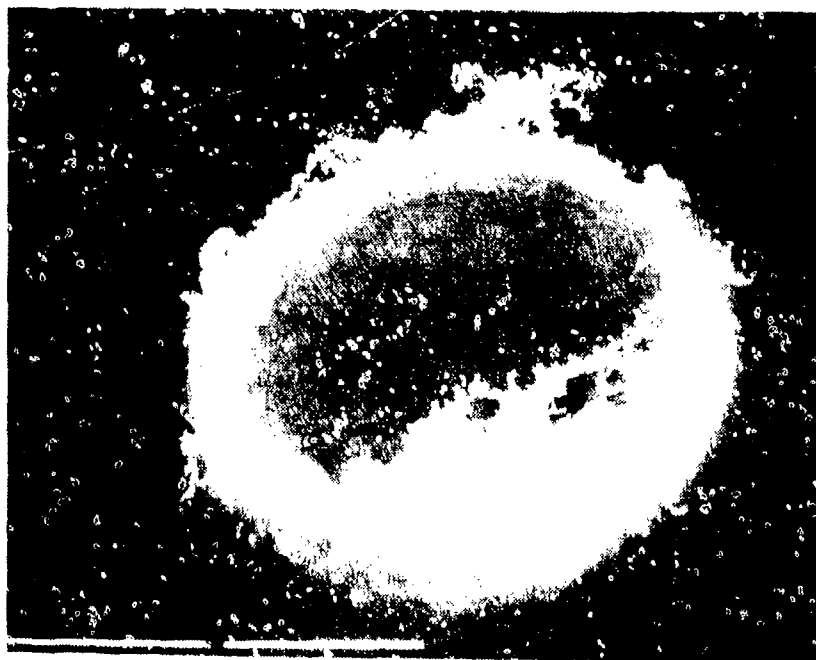
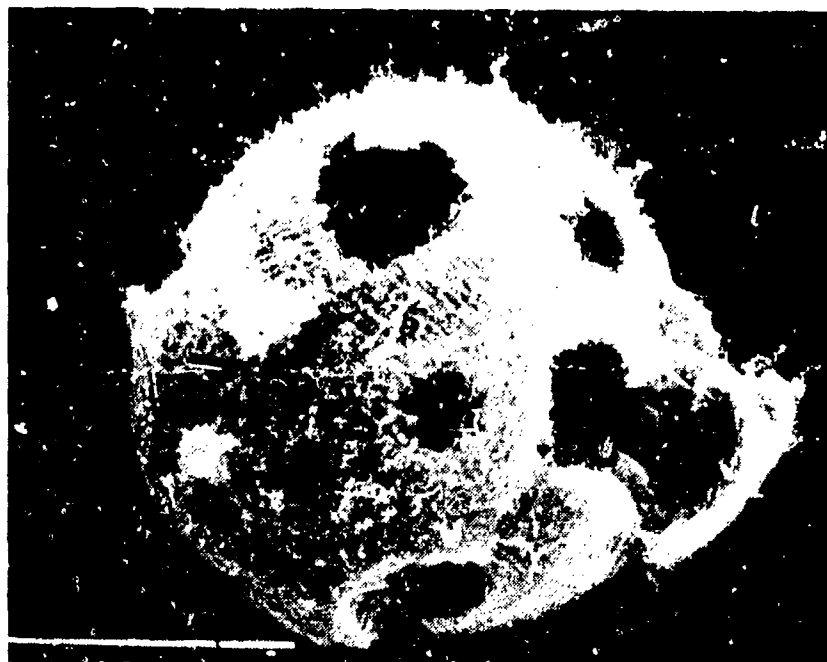


Figure 9. Hollow Particle Demonstrating Variable Wall Thickness: Bar Represents 5  $\mu\text{m}$



(High iron content of this particle is indicated by crystal formation, particularly along inner wall surface)

Figure 10. Perforated, Hollow Sphere; Bar at Right Represents 5  $\mu$ m

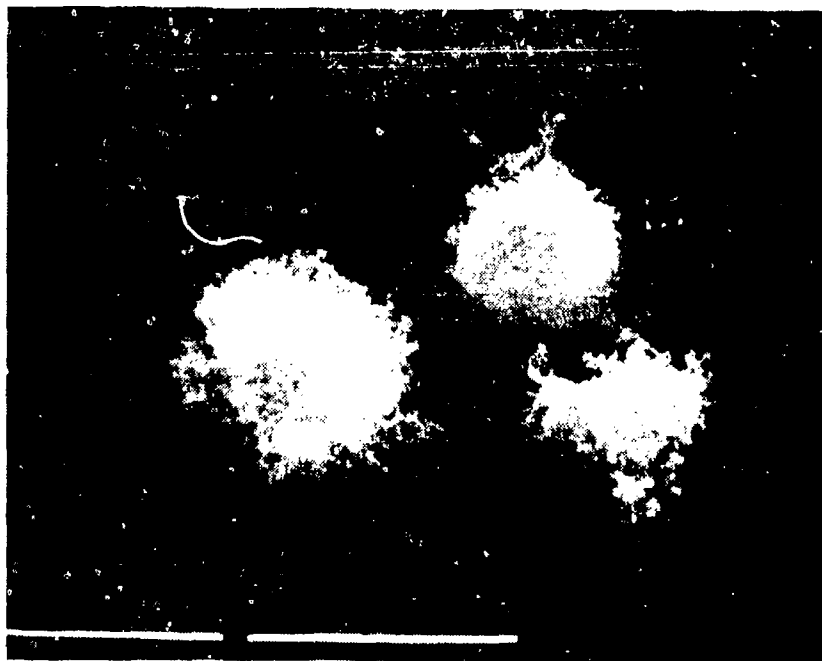
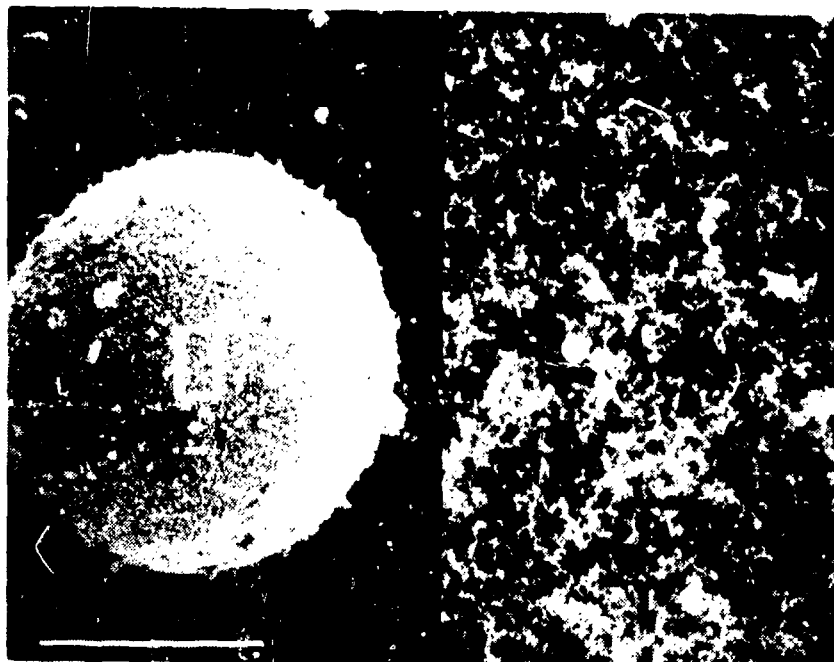


Figure 11. Several Airborne Particles Demonstrating Surface Coverage by Ultrafine Particulates; Bar at Right Represents 5  $\mu$ m



(Note ultrafine particulates are evenly distributed upon the surface)

Figure 12. Dual Magnification (10X) of a Staballoy and Iron Particle; Bar Represents 55.5  $\mu\text{m}$  at Lower Magnification

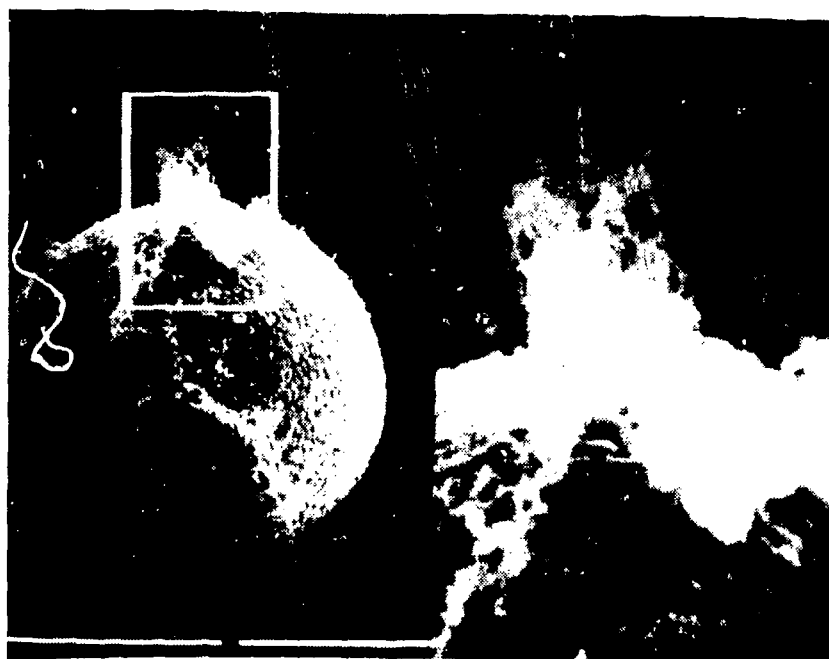


Figure 13. Flaring of an Ultrafine Aggregate from the Surface of an Airborne Particle Shown in Dual Magnification (3X); Bar at Right Represents 5  $\mu\text{m}$  Lower Magnification

This property of adhesion or coalescence is particularly evident in Figure 14 which shows two depleted uranium particles interconnected by a single, almost invisible, strand of material comprised entirely of ultrafine particulates.

Although generally found in association with larger particles, the ultrafine particulates were also detected in the free state directly upon the surface of the collective tape. At low magnification these particulates appeared as large concentric masses often reaching several hundred micrometers in diameter (Figure 15). At greatly increased magnification (Figure 16), these masses were revealed as consisting of vast numbers of small aggregates and long angular chains. The ultrafine spherical particles comprising these aggregates measured approximately 0.01 to 0.1  $\mu$ m in diameter.

#### PARTICLES ISOLATED FROM SOIL SAMPLES

Samples collected from the soil near the target site were separated according to size and density by a multistep preparative procedure. This technique proved beneficial in that it resulted in the exclusion of low density materials such as sand and clay as well as particles larger than those required for this study.

An overall view of particles isolated from soil is shown in Figure 17. The use of porous, polycarbonate membranes as a supporting material resulted in well dispersed samples. The degree of dispersion was readily controlled and was dependent only upon initial particle concentration.

Morphology of particles removed from soil samples was quite unlike that of their airborne counterparts. Far greater numbers of irregularly shaped fragments were present, presumably the result of interaction and fusion with sand and other materials within the soil (Figure 18). Spherical particles, although quite numerous, generally lacked the convoluted surface morphology so apparent in airborne samples. Their surfaces were consistently smoother and frequently speckled with knobby blebs (Figure 19). Some of these blebs were clearly continuous with the surrounding surface whereas others appeared nearly detached.

The relative fragility of these uranium particles was clearly evident following brief exposure in the laboratory to ultrasound (Figure 20). Although sonification lasted no longer than 15 seconds, particles showed extensive fracturing and in many instances complete disintegration.

#### PARTICLE COMPOSITION

The elemental composition of individual particles was qualitatively determined by energy dispersive X-ray spectroscopy. Depleted uranium particles frequently contained iron, aluminum, silicon, calcium, magnesium, potassium, titanium, and tungsten as a result of contamination during impaction and settling.

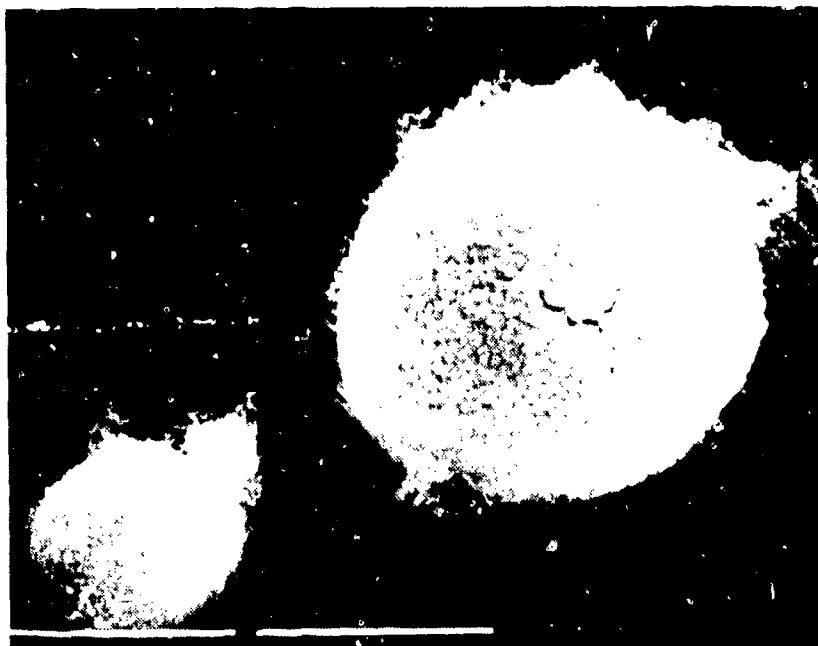


Figure 14. Ultrafine Particulates on the Surface of Staballoy Particles Showing Interconnecting Thread; Bar at Right Represents 5  $\mu\text{m}$

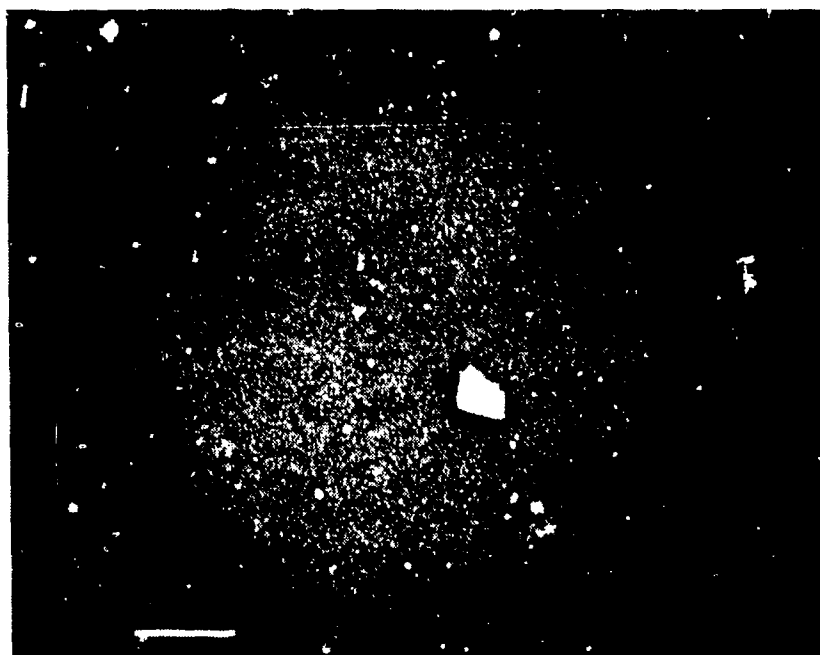
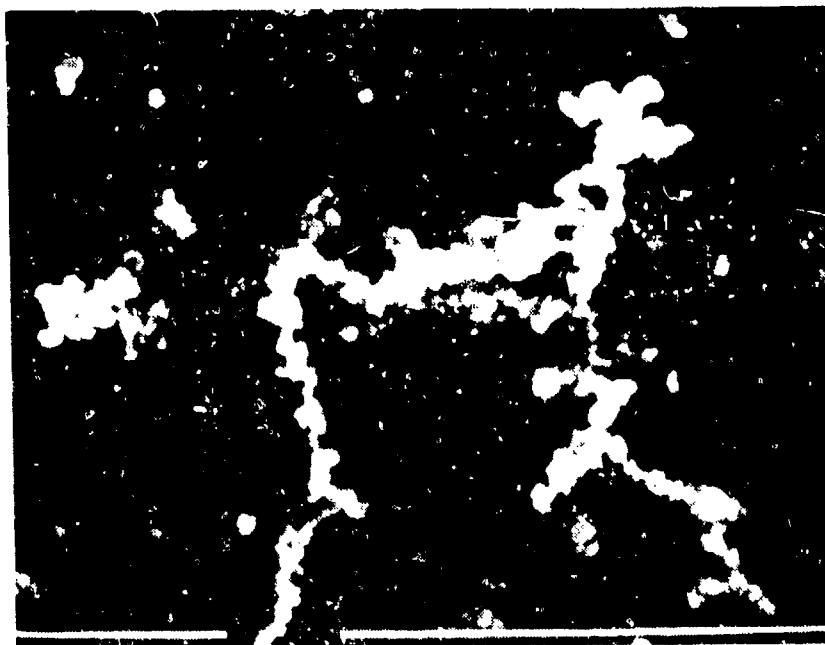


Figure 15. Concentric Pattern of Free Ultrafine Particulates on Double-Stick Tape; Bar Represents 55.5  $\mu\text{m}$



(Same material shown in Figure 15)

Figure 16. High Magnification Showing Aggregation of Ultra-fine Particles; Gap Between Bars Represents  $0.5 \mu\text{m}$

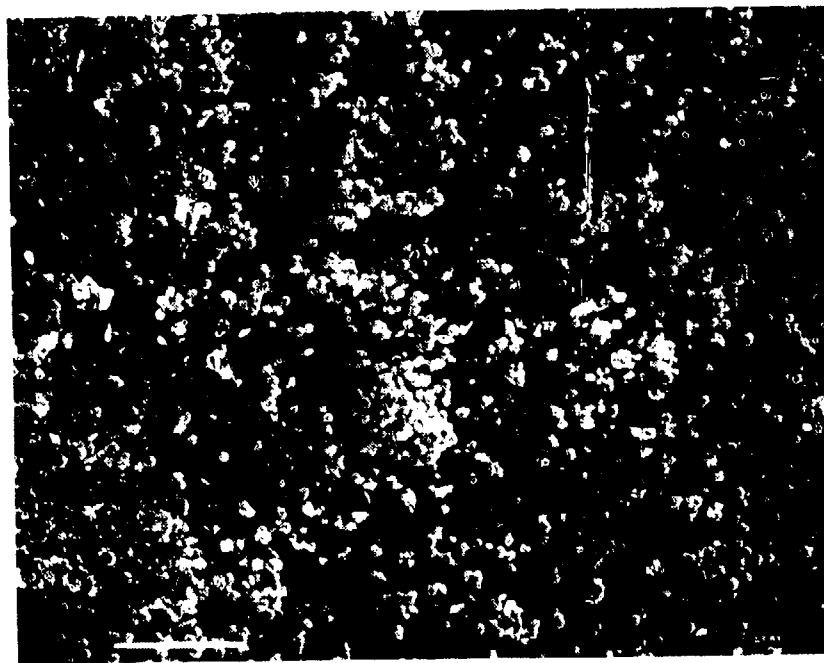


Figure 17. Soil Particles of Density Greater Than 4.3 Which Passed Through a  $12 \mu\text{m}$  Polycarbonate Nuclepore Membrane; Bar Represents  $55.5 \mu\text{m}$

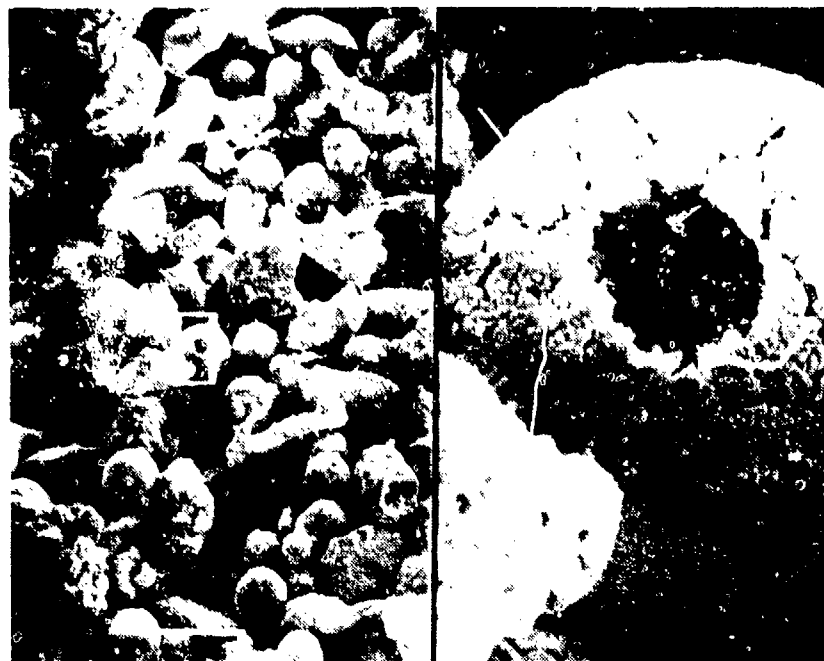


Figure 18. Dual Magnification (10X) of Soil Particles Revealing Both Spherical Particles and Fragments; Bar Represents 55.5  $\mu\text{m}$  at Lower Magnification

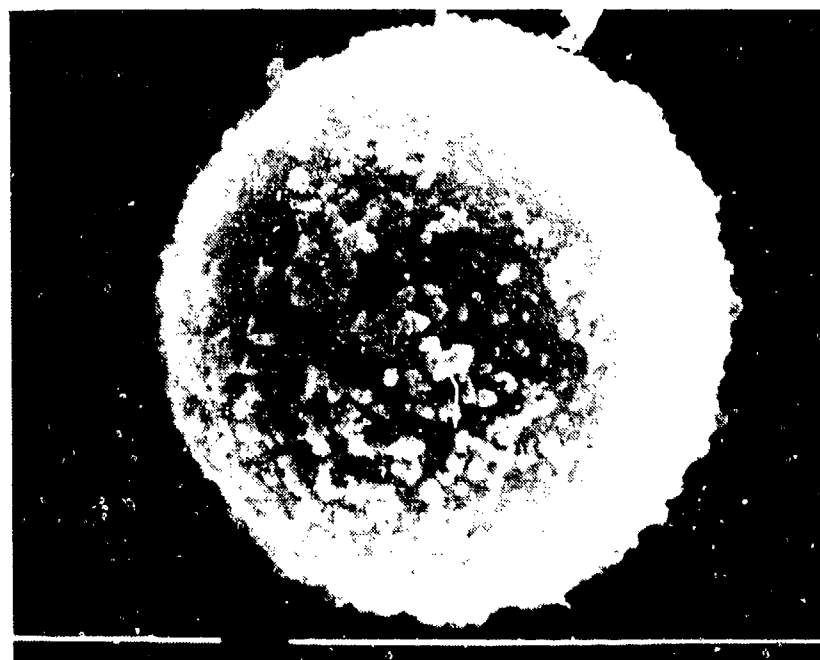


Figure 19. Knobby Soil Particle; Gap Between Bars Represents 0.5  $\mu\text{m}$

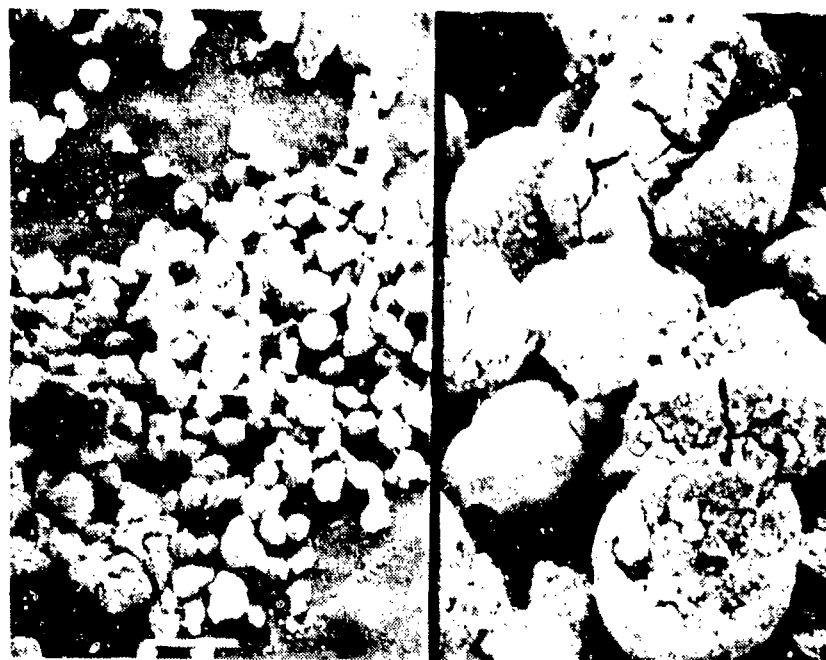


Figure 20. Dual Magnification (5X) of Particle Breakup Due to  
15 Second Exposure to Ultrasound; Bar Represents 55.5  $\mu\text{m}$   
at Lower Magnification



## SECTION IV

### TECHNICAL SUMMARY

Although a number of heavy metals have been fabricated in high density projectiles in an attempt to increase the effectiveness of armor piercing munitions in recent years, depleted uranium has been used most extensively. Selection of depleted uranium as the most desirable of the candidate materials was based primarily upon its (1) high density, (2) pyrophoricity, (3) metallurgical properties, (4) availability, and (5) relatively low cost.

The medical and environmental implications of depleted uranium have been widely studied (References 4 and 5). Biotic hazards, generally considered to be low and resulting only after prolonged exposure, are believed to be due primarily to its chemical rather than radiological properties. But even with the vast amount of physiological data already acquired, additional research is necessary to better define the physical and chemical nature of fragmentary depleted uranium generated as a consequence of its use in military weaponry. Foremost attention should be focused on its potential for dissemination within the environment and entry into biological systems, particularly that of man.

In a recent report, Hanson et al (Reference 6), demonstrated the formation of particulate aerosols following penetration of depleted uranium projectiles into armor plate targets. This study was especially valuable in that the overall aerodynamic characteristics and size distribution of uranium particles were defined.

The present study was undertaken to examine the gross morphological characteristics of these particulates. Such specific knowledge is required for determination of potential safety hazards associated with the respiration and deposition of uranium aerosols within the lungs. Particles in the 0.1- to 0.5- $\mu$ m size range are of greatest concern because of their high efficiency for deposition in the lungs. This range has been defined appropriately as the respirable size range.

For this study, 105 mm rounds, each containing approximately 3.5 kg depleted uranium, were fired at multiple steel plate targets. Airborne particulates were collected on double-stick tape through a combination of settling, impaction, thermal precipitation, and diffusion. However, due to the pyrophoric nature of depleted uranium and the high projectile velocity attained, the predominant mechanism appeared to be impaction. A relatively high collection efficiency was anticipated for all but the larger fragments due to the proximity of sampling sites to the target.

Scanning electron microscopy revealed that airborne particulates were primarily spherical, the surfaces of which were highly convoluted. Particles were at times comprised of partially overlapping, concave plates, formed as a result of polyfocal solidification. Extensive fracturing, particularly

along the convoluted folds and plate lines, accounted for the apparent fragility associated with airborne particles of the rugose type. Under normal weathering conditions such particles could be expected to break up rapidly, thereby contributing to an increase in the total number of respirable-size particles.

Particle disintegration would be further accelerated by the hollow nature of many of the spheres. Hollow particles, which are frequently thin-walled or perforated, are extremely vulnerable to weathering and thus subject to rapid deterioration.

The apparent fragility of the rugose, hollow, and perforate particles was further substantiated through observation of soil particulates. These samples contained material which had accumulated over many months of testing and therefore represented aged particulate debris. The relatively low incidence of these types of particles in soil must be attributed to their inherent instability and results in rapid weathering and subsequent formation of smaller particulates.

An unexpected phenomenon was the formation of ultrafine particles less than 0.1  $\mu\text{m}$  in diameter. These particulates, generally observed adhering to the surfaces of larger particles, presumably were formed as a result of the extreme temperatures achieved and the highly reactive nature of pyrophoric depleted uranium. These ultrafine particles exhibited an extreme tendency to coalesce, probably due to spontaneous diffusion charging. This coalescing tendency of particles, which were originally below the respirable size-range, is especially significant since it resulted in the formation of abundant agglomerates that fell within the respirable range.

The elemental composition of individual particles was qualitatively determined by non-destructive X-ray spectroscopy. Airborne particles were comprised primarily of alloyed uranium and iron. Although the ratio of the two metals varied considerably among particles, the fact that alloying did occur is consistent with the violent interaction between penetrator and target at impact.

Particles isolated from soil samples near the target area, in addition to uranium and iron, frequently contained appreciable amounts of silicon, aluminum, and/or tungsten. Fusion with both silicon and aluminum had been anticipated as a result of interaction with sand and clays within the soil. The presence of tungsten was due to contamination of the target site from previous test firings of high density penetrators employing that material.

This study has shown that scanning electron microscope techniques are ideal for examination of particles formed from the impact of depleted uranium projectiles against armor plates. Results show that appreciable quantities of respirable-size particles are released during use of these projectiles. Although particles are initially formed over an extremely broad size range, eventual weathering of large particles together with coalescence of ultrafine particles combine to increase the potential total number of particulates within the respirable range.

#### REFERENCES

1. Leibowitz, L., L. Baker, J.C. Schnizlein, L.W. Mishler, and J.P. Bingle, "Burning Velocities of Uranium and Zirconium in Air" in Nuclear Science and Engineering, 15:395-403, 1963.
2. Physics of High Speed Impact, Final Summary Report, PATEC-TR-157-70, July 1970.
3. McCrone, W.C., and J.G. Delly, The Particle Atlas, Volume 3, Ann Arbor Science Publishers, Inc., Ann Arbor, Michigan, 1973, pp. 773-779.
4. Medical and Environmental Evaluation of Depleted Uranium, Volume I, JTCG/ME Ad Hoc Working Group for Depleted Uranium, 1974.
5. Hodge, H.C., J.N. Stannard, J.B. Hursh, Uranium, Plutonium, Transplutonic Elements, Springer-Verlag Publishers, New York, 1973.
6. Hanson, W.C., J.C. Elder, H.J. Ettinger, L.W. Hantel, and J.W. Owens, Particle Size Distribution of Fragments from Depleted Uranium Penetrators Fired Against Armor Plate Targets, LA-5654 Los Alamos Scientific Laboratory, 1974.

# INITIAL DISTRIBUTION

|                                  |    |
|----------------------------------|----|
| ASD/ENFEA                        | 1  |
| Hq USAF/SAMI                     | 1  |
| OO-ALC/MMWP                      | 2  |
| AFIS/INT                         | 1  |
| Hq TAC/DRA                       | 1  |
| TAC/INAT                         | 1  |
| ASD/ENESH                        | 1  |
| USA TRADOC Sys Analy Act/ATAA-SL | 1  |
| Hq USAFE/DOQ                     | 1  |
| Hq PACAF/DOOFQ                   | 1  |
| ASD/XRP                          | 1  |
| COMIPAC/I-232                    | 1  |
| AFATL/DLODL                      | 2  |
| DDR&E (Tech Lib)                 | 1  |
| USAF/DFCBS                       | 1  |
| Dugway Prov Gd/Tech Lib          | 1  |
| AFLC/MMNO                        | 1  |
| SAAMA/SFQT                       | 1  |
| AFSC/SDW                         | 1  |
| Hq USAF/RDP                      | 1  |
| AFSC/DEV                         | 1  |
| DDR&E/Env & Life Sciences        | 1  |
| DRDAR-CLJ-L                      | 1  |
| USAF (Env Health Lab)            | 1  |
| NWC Env Eng                      | 1  |
| AMD/RD                           | 1  |
| AMRL/THE                         | 1  |
| AMRL/THT                         | 1  |
| ADTC/CSV                         | 1  |
| ADTC/SGPE                        | 1  |
| Det 1 (CEEDO/EC)                 | 1  |
| AJL/LSE 71-249                   | 1  |
| AFLC/DS                          | 1  |
| ADTC/DEN                         | 1  |
| US Army Natick Lab               | 1  |
| ADTC/DLV                         | 20 |
| Los Alamos Sci Lab, H-12         | 1  |
| DDC/DDA                          | 2  |
| Deseret Test Ctr/Tech Lib        | 1  |
| NWC/Tech Lib                     | 1  |
| AEDC/DEE                         | 1  |
| AFCEC/EO                         | 1  |
| ARRADCOM/DRDAR-SCM-P             | 1  |
| Battelle Pacific Northwest Lab   | 1  |